Combustion and Flame 201 (2019) 65–77

Contents lists available at ScienceDirect

Combustion and Flame

journal homepage: www.elsevier.com/locate/combustflame

A conceptual model of the flame stabilization mechanisms for a lifted Diesel-type flame based on direct numerical simulation and experiments

Fabien Tagliante[a,*], Thierry Poinsot[b], Lyle M. Pickett[c], Perrine Pepiot[d,e], Louis-Marie Malbec[a], Gilles Bruneaux[a], Christian Angelberger[a]

[a] *IFP Energies Nouvelles, 1 et 4 avenue de Bois-Préau Institut Carnot IFPEN Transports Energies, Rueil-Malmaison Cedex, 92852, France*
[b] *IMFT (Institut de Mécanique des Fluides de Toulouse), 2 Allée Camille Soula, Toulouse 31400, France*
[c] *Combustion Research Facility, Sandia National Laboratories, P.O. Box 969, MS 9053, Livermore, CA 94551, USA*
[d] *CERFACS,42 Avenue G.Coriolis,Toulouse Cedex, France*
[e] *Sibley School of Mechanical and Aerospace Engineering, Cornell University, NY 14853, USA*

ARTICLE INFO

Article history:
Received 8 October 2018
Revised 8 November 2018
Accepted 7 December 2018
Available online 20 December 2018

Keywords:
DNS
Lift-off length
Flame stabilization
Auto-ignition
Triple flame
Diesel combustion

ABSTRACT

This work presents an analysis of the stabilization of diffusion flames created by the injection of fuel into hot air, as found in Diesel engines. It is based on experimental observations and uses a dedicated Direct Numerical Simulation (DNS) approach to construct a numerical setup, which reproduces the ignition features obtained experimentally. The resulting DNS data are then used to classify and analyze the events that allow the flame to stabilize at a certain Lift-Off Length (LOL) from the fuel injector. Both DNS and experiments reveal that this stabilization is intermittent: flame elements first auto-ignite before being convected downstream until another sudden auto-ignition event occurs closer to the fuel injector. The flame topologies associated to such events are discussed in detail using the DNS results, and a conceptual model summarizing the observation made is proposed. Results show that the main flame stabilization mechanism is auto-ignition. However, multiple reaction zone topologies, such as triple flames, are also observed at the periphery of the fuel jet helping the flame to stabilize by filling high-temperature burnt gases reservoirs localized at the periphery, which trigger auto-ignitions.

1. Introduction

The stabilization of diffusion flames remains one of the main challenges of combustion science [1]. Triple flames have been identified as a main phenomenon contributing to the stabilization of lifted diffusion flames created between two cold streams of fuel and oxidizer [2–4]. However, when one of the two streams is hot, as in Diesel fuel sprays, auto-ignition events do certainly also play an important role [5–9] and interact with triple flames [10]. In such configurations (referred to as Autoignitive Conditions Diffusion Flames, or ACDF), a fuel jet is injected into hot air. The distance at which the flame stabilizes from the fuel injector nozzle, called LOL for Lift-Off Length, has been shown to play a major role in the soot formation processes [5,6,11,12], and its precise prediction would require a detailed understanding of all the interacting mechanisms controlling it. Considering the difficulty to distinguish the flame stabilization mechanisms experimentally [13], DNS (Direct Numerical Simulation) has been used to address this question. Krisman et al. [10] have been the first to identify triple flames interacting with low-temperature chemistry upstream of them based on a laminar, two-dimensional, stabilized DME flame studied by DNS. This same methodology has been used by Dalakoti et al. [14] and Deng et al. [15,16], who confirmed the importance of triple flames under Diesel conditions by studying the impact of inlet temperature [15] and velocity [16]. These studies were followed by a 3D DNS of a turbulent lifted DME slot gaseous jet flame performed by Minamoto and Chen [17], which confirmed the presence of triple flames under Diesel conditions. They characterized the local reaction zone structure at the lift-off as predominantly being a deflagration rather than resulting from auto-ignition. These observations have been confirmed by Shin et al. [18] through post-processing of their DNS based on fluid age analysis.

The objective of the present work was to perform a DNS study of the spatial and temporal evolution of a Diesel-type spray previously studied experimentally [19] in order to explore in detail the phenomena contributing to the spray-flame stabilization.

---

[*] Corresponding author.
E-mail address: fabien.tagliante@ecp.fr (F. Tagliante).

https://doi.org/10.1016/j.combustflame.2018.12.007

Ideally, such a DNS would have to simulate the full spray, including in particular the liquid fuel spray originated from the injector nozzle. A DNS including the latter would be a challenge in itself and has not been addressed by published research due to its inherent complexity and extreme requirements in terms of spatial and temporal resolution. Published DNS have therefore restricted the computational domain to the gaseous part of the spray where chemical reactions essentially take place. A first approach was to perform temporal DNS of the turbulent mixing layer created downstream of the liquid part of the spray [20–23]. While this allowed addressing realistic Damköhler numbers, it may not account for spatial recirculation of hot burnt gases that have been found to possibly be of importance for the flame stabilization of ACDF [6]. Another type of DNS simulated a spatially stabilized gaseous flame set up to be as representative as possible to Diesel-spray conditions [17]. While this allowed addressing Damköhler numbers under Diesel-spray conditions, the studied Reynolds numbers were considerably smaller than that of a Diesel spray.

In the present work, we chose to perform a DNS of the spatial evolution of the gaseous part of the spray studied in [19] (α condition), in order to account both for realistic Reynolds and Damköhler numbers, and to address in particular the recirculation of burnt gases and their suspected impact on flame stabilization. To limit the computational cost of such an approach, the simulations were restricted to 2D, which allowed ensuring a sufficient resolution of the small spatial scales of premixed flames under the studied conditions.[1]

Unlike many turbulent flames, which can be computed with simplified chemical descriptions [24,25], the simulation of ACDF requires more complex chemical kinetics. The LOL time evolution is a discontinuous quantity, characterized by frequent jumps when the flame auto-ignites. Experiments reveal that these auto-ignition events (called “Events A” in [19]) are followed by the formation and the downstream convection of flames (called “Evolution B” [19]) before a new auto-ignition event occurs upstream and brings the flame back closer to the injector. Low-temperature chemistry has been shown to play an important role in that dynamic process [19]. Reproducing these low-temperature chemistry phenomena, especially in the NTC (Negative Temperature Coefficient) regime, is impossible with global schemes [22] and requires more complex chemistry descriptions.

In the present DNS, chemistry was modelled using an ARC (Analytically Reduced Chemistry) scheme [26–30] adapted for n-dodecane / air flames at 3.4 MPa.

The paper is organized as follows: the computational domain and numerical method employed in the DNS of the ACDF configuration is described in Section 2, followed by the chemical scheme reduction methodology and its validation in Section 3. The analysis tools, used to identify the instantaneous LOL as well as the local reaction zone topologies around it, are detailed in Section 4. Then, Section 5 presents a comparison between experiments [19] and the performed DNS in order to validate the strong hypothesis and in particular those related to a 2D simulation and a synthetic simplified turbulence at the inflow of the gas jet allow realistic predictions. In Section 6, each discrete instantaneous lift-off predicted by the DNS is identified to be either of the Event A or Evolution B types following the definitions proposed in [19]. Furthermore, the developed automatic tools analysis are used to identify the local reaction zone topologies around discrete instantaneous lift-off positions. Finally, a conceptual model for flame stabilization in ACDF-type configurations is proposed in Section 7 based on the performed analyses and resulting observations.

2. Configuration

The case simulated in the present work had previously been studied experimentally. Details on the employed techniques and obtained results can be found in [19], where it is referred to as the α condition.

The configuration consists of a n-dodecane liquid fuel injected into a large constant volume vessel containing a mixture with a 16% (by volume) oxygen concentration, at an initial pressure of 3.4 MPa and temperature of 800 K.

2.1. Simplifying assumptions

Performing a 3D DNS of the full liquid spray, and its combustion under such Diesel engine-like conditions, would require a very fine spatial and temporal discretization in order to capture the smallest scales. An estimation of the resulting necessary computational effort indicated that the cost of performing such a 3D DNS would be prohibitive.

In order to define an affordable computational framework able to reproduce essential aspects of ACDF flame stabilization, the following simplifying assumptions were made:

- The simulation was simplified to be two-dimensional. Despite the related limitations, in terms of an accurate reproduction of all features of a turbulent flow, comparisons with experimental findings indicated that this strong simplification allowed capturing key features at a fraction of the cost of a 3D DNS. It also simplified the analysis of the reaction zone dynamics significantly.
- As experimental observations for the simulated condition showed a flame stabilization downstream of the zone where the liquid spray impacts the local flow dynamics, the liquid injection was not included in the simulations. As shown in Fig. 1, the computational domain was therefore started 20 mm downstream the injector outlet, i.e. downstream of the liquid length that was estimated to be 18 mm [31].
- The computational domain was chosen to include an area of interest axially situated between 25 mm and 50 mm downstream of the injector. As illustrated in Fig. 1 (top), experimental findings [19] indicate that this well-resolved area of interest includes the spatially relatively stable low-temperature-chemistry (e.g. formaldehyde), as well as the region situated axially between 26 and 45 mm downstream the injector in which the LOL varies. In the radial direction, the area of interest encompasses a region containing high-temperature products localized at the jet periphery, which, according to [6], may contribute to the flame stabilization.
- Inflow boundary conditions imposed in the central part of the jet were not chosen to reproduce the complex turbulent multi-species and possibly reactive flow found at that axial position 20 mm downstream the injector. These complex flow conditions are not known from published research, and would indeed require performing a full DNS of the spray. The inflow boundary conditions were thus strongly simplified to only reproduce the mean mass flow rate and a very approximate level of velocity fluctuations. Temperature fluctuations were neglected, and only a non-reactive mixture of fuel and air was fed into the domain. Such inflow conditions are very crude approximations, but the flow can develop between the inflow and the beginning of the area of interest at 25 mm, where we observed a qualitatively realistic turbulent reactive flow. This was checked quantitatively in a posteriori way by comparing DNS predictions with experimental findings, as will be exposed in Section 5. In this sense, the inflow boundary conditions should be viewed only as a crude simplification resulting from the

---

[1] Care was taken to base the 2D DNS of the gaseous part of the spray on a sufficiently realistic chemical mechanism including low-temperature chemistry.

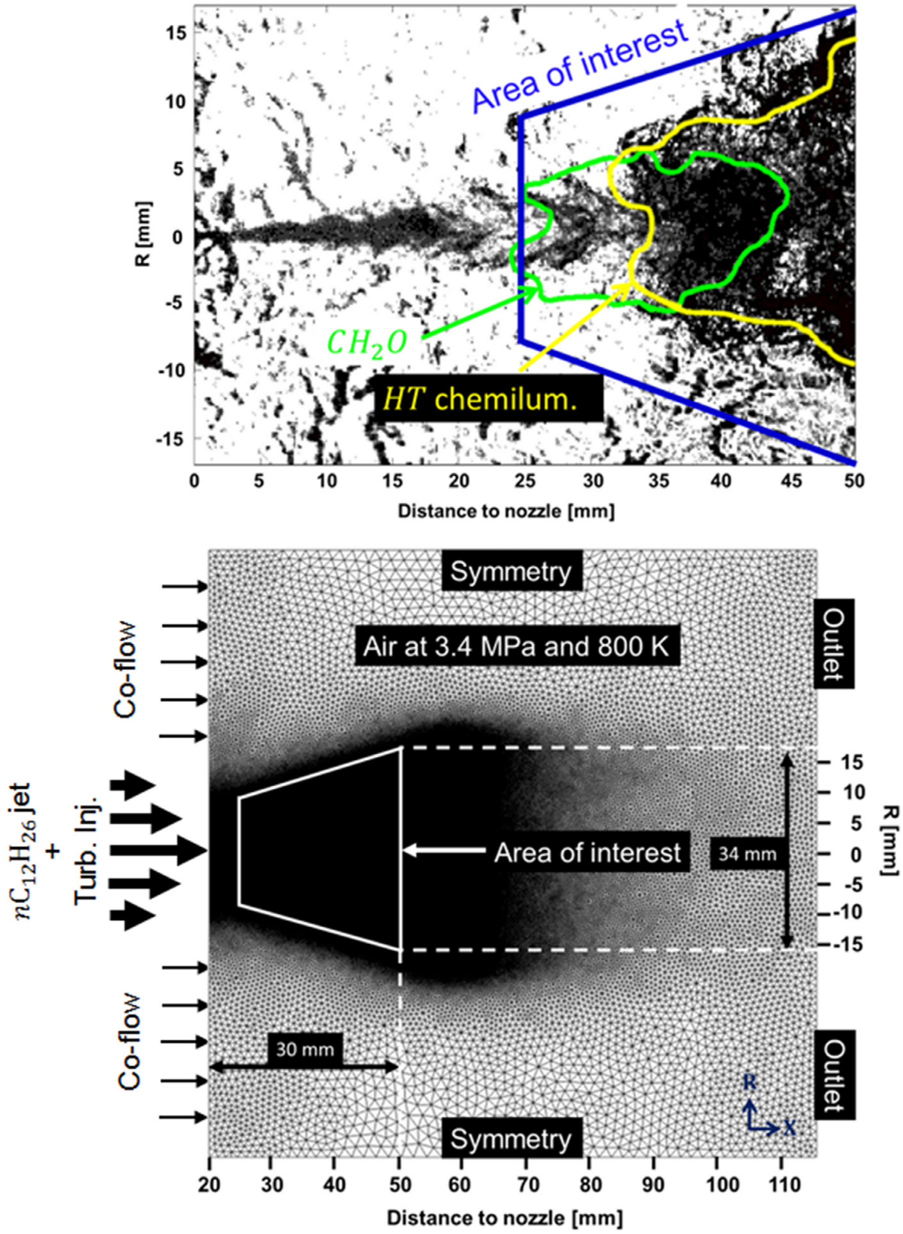

Fig. 1. Top: Superposition of the gas envelope of the spray (Schlieren imaging) on an iso-contour of the formaldehyde cloud (green line, high-speed 355 LIF), and the high-temperature flame (yellow line, broadband chemiluminescence). This image was obtained from the experimental setup presented in [19]. Bottom: Computational domain showing the used tetrahedral grid which is refined in the area of interest to capture combustion phenomena.

absence of detailed knowledge, and chosen to allow for realistic flow conditions in the area of interest to which all analysis presented below were restricted.

- Only the "quasi-steady" state reached once the spray flame has auto-ignited was studied [32]. This phase is characterized by a constant mean fuel flow rate.

In Section 5, the DNS will be compared to experimental findings in order to a posteriori assess the validity of these assumptions.

2.2. Numerical set-up

The present DNS were performed with the AVBP code co-developed by CERFACS and IFPEN [33]. AVBP solves the compressible reactive Navier-Stokes equations for momentum, total energy, and species mass fractions on unstructured grids. The Lax-Wendroff scheme [34] (second-order accurate in space and time) was used.

Figure 1 (bottom) shows the 2D square computation domain. Spatial discretization is based on an unstructured tetrahedral mesh. The highest spatial resolution of 6 µm is imposed in the area of interest that covers the region where key mechanisms of flame stabilization take place and were analyzed. This cell size was chosen to achieve a sufficient resolution of the estimated premixed flame thickness under the simulated conditions, as outlined in Section 3.2. The cell size is progressively coarsened laterally and downstream of the area of interest in order to impose lateral and downstream boundary conditions far enough to mimic the large size of the real constant volume vessel used in the experiments. The resulting mesh comprises 33.7 million nodes. The time-step

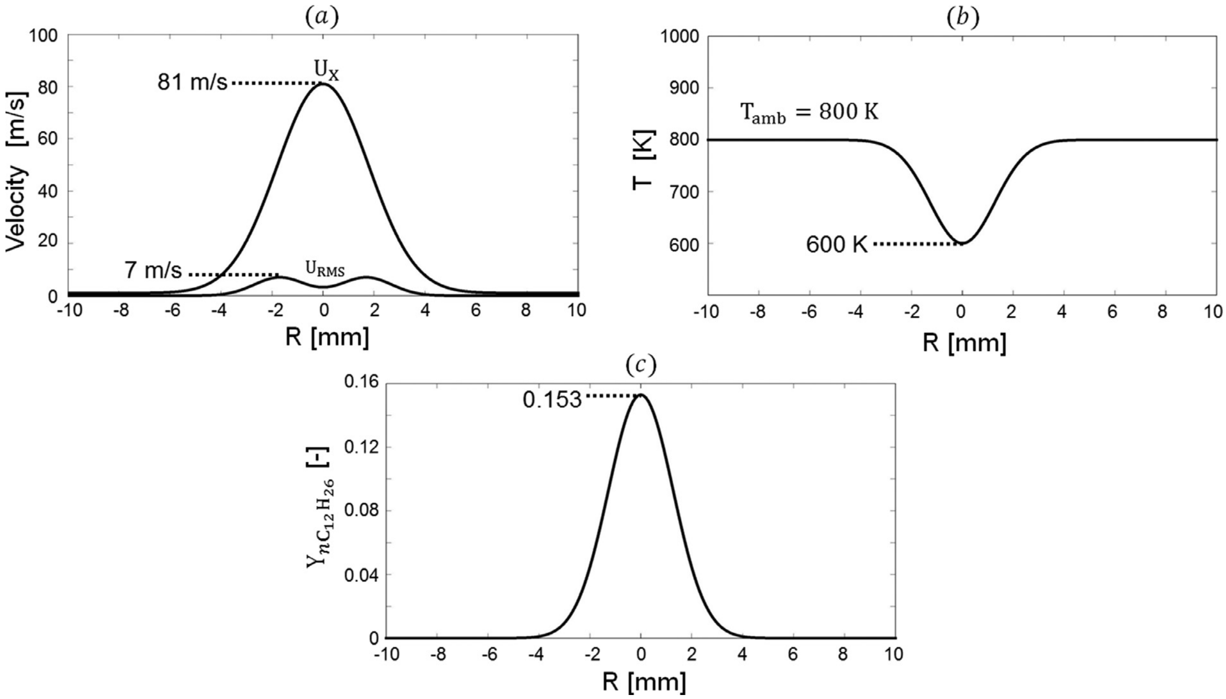

Fig. 2. All of the graphs show radial profiles imposed at the inlet boundary condition. (*a*): Axial flow velocity (U_X) and axial velocity fluctuation (U_{RMS}), (*b*): temperature, (*c*): n-dodecane mass fraction.

was 1.9 ns to satisfy the acoustic Courant-Friedrichs-Lewy (CFL) condition of the explicit time advancement.

Lateral symmetric boundary conditions are used. The inlet and outlet boundary conditions are imposed using the Navier-Stokes characteristic boundary condition (NSCBC) [35]. At the outflow, a relaxation method is used to impose the vessel pressure of 3.4 MPa while minimizing spurious wave reflections.

In the central part of the inflow boundary, an relaxation method is used to impose the mean profiles of axial velocity (U_X), temperature (T) and species mass fractions (Y_k). These profiles, shown in Fig. 2 (and detailed in Appendix 1), impose the constant mean gas flow entering the computational domain as a result of the not simulated upstream liquid spray during quasi-steady state.

In order to roughly approximate the turbulence entering the domain as a result of the upstream spray, temporal fluctuations (following the Taylor hypothesis), proportional to the U_{RMS} profile (shown in Fig. 2), are added to the axial in-flow velocity using the Celik method [36] and following the Passot Pouquet spectrum [37] as detailed in Appendix 1.

A co-flow of $U_{coflow} = 1m/s$ is imposed laterally of the central inflow to avoid negative axial velocities on the inlet, which could cause numerical difficulties. This small velocity is assumed to have a negligible impact on the stabilization mechanism.

The random perturbations, added to the mean axial inflow velocity, were selected to achieve a satisfactory opening angle of the jet in the area of interest. This was checked by performing a non-reactive simulation and comparing time-averaged radial profiles of velocity, temperature, and fuel mass fraction obtained by post-processing instantaneous DNS fields with profiles given by experimentally established correlations. This allowed (not shown here) to check that the imposed boundary conditions yielded satisfactory mean profiles in the area of interest where flame stabilization mechanisms were studied. Therefore, the chosen inflow boundary conditions allow to investigate the flame stabilization mechanisms, unlike temporally developing jets created by a mixing layer between fuel and air [20–23].

Table 1
Initial species mass fractions in the vessel.

Species	N_2	O_2	CO_2	H_2O	$nC_{12}H_{26}$
Mass fraction [-]	0.7016	0.1746	0.1001	0.0237	0

The initial condition for the DNS was a flow at rest at the initial temperature, pressure and composition known from the experiments. The initial mass fractions of N_2, O_2, CO_2, and H_2O are imposed to be spatially homogeneous and equal to the values given in Table 1. The CO_2 and H_2O species are products of the lean pre-combustion used in the experiments to bring the vessel to its initial conditions at the start of injection.

The simulated physical time was 12 ms. A first initial phase of 3 ms was necessary to have the flame ignite and for the flow to reach a stabilized state in the mean. Flame stabilization was only analyzed after this initial stage.

The computational cost was 120,000 CPU hours per simulated physical millisecond. AVBP allowed achieving a return time of approximately 24h per simulated millisecond on 4992 cores.

3. Chemical mechanism

The reference chemical kinetics scheme used in this work is the 54-species skeletal model for n-dodecane oxidation developed by Yao et al. [38], itself based on the detailed kinetic scheme for a variety of alkanes by Sarathy et al. [39].

3.1. Development of the reduced scheme

This reference mechanism is further reduced for the conditions relevant to the DNS presented here using the YARC reduction tools [26]. The resulting analytically reduced chemistry (ARC) model is then validated against experimental and simulation data obtained using Yao's model. Comparison are shown in Fig. 3 for laminar flame speed (left column) and auto-ignition delay (right

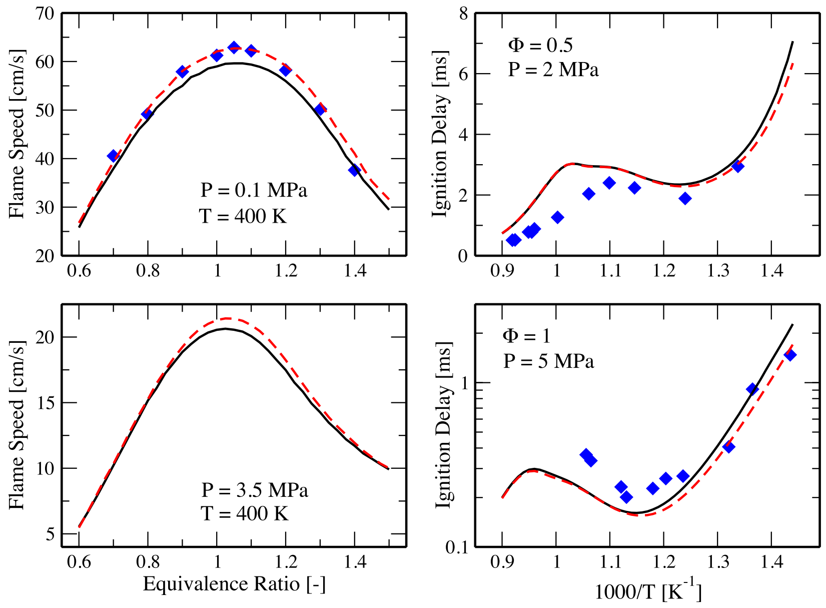

Fig. 3. Comparison between the reference mechanism of Yao et al. (solid black lines, [38]) the ARC model derived in the work (dotted red line), and experimental data (symbols, [41–43]). Left: laminar flame speeds, right: ignition delay times.

Table 2
Summary of the reduced mechanism (28 ARC): transported (left) and Quasi Steady State (QSS) (right) species.

Transported species (28)	QSS species (19)
$N_2, O, H_2,$ $H, OH, H_2O,$ $H_2O_2, O_2, HO_2,$ $CH_2O, CO_2, CH_3,$ $CO, C_2H_6, CH_4,$ $C_2H_4, C_2H_2, C_3H_6,$ $C_4H_8, C_5H_{10}, C_6H_{12},$ $C_7H_{14}, C_8H_{16}, C_9H_{18},$ $C_{10}H_{20},\ C_{12}H_{25}O_2,\ n-C_{12}H_{26},$ $OC_{12}H_{23}OOH$	$CH_2,\ HCO,\ CH_2^*,$ $CH_3O, C_2H_3, CH_2CHO,$ $C_2H_5,\ a-C_3H_5,\ C_2H_3CHO,$ $n-C_3H_7,\ C_4H_7,\ p-C_4H_9,$ $p-C_5H_{11},\ p-C_7H_{15},\ p-C_{12}H_{25},$ $s3-C_{12}H_{25},\ s-C_{12}H_{25},\ C_{12}OOH,$ $O_2C_{12}H_{24}OOH$

column). Laminar premixed flame values were obtained for equivalence ratios in the range 0.7–1.3 for atmospheric and high pressure (3.5 MPa). Auto-ignition delays are checked for pressures of 2.0–5.0 MPa, equivalence ratios of 0.5–1.2, and initial temperatures of 700–1200 K. The first step of the reduction methodology is to identify species and reactions which can be removed without affecting the laminar flame speed and the auto-ignition delay using the directed relation graph method with error propagation [27]. At the end of this stage, 7 species are removed. Species for which a Quasi-Steady State Approximation (QSSA) can be used are, then, chosen using the Level Of Importance criterion [40]. The resulting ARC scheme is composed of 28 transported species, 19 QSS species (Table 2) and 198 reactions. As shown in Fig. 3, the 28-species reduced scheme correctly reproduces the laminar flame speeds and the auto-ignition delays over the selected range of conditions, also capturing the NTC region for a fixed composition with varying temperature.

3.2. Estimation of the thermal flame thickness

The reduced scheme was used to estimate the necessary spatial resolution in the area of interest of the computational domain. To this purpose, a 1D premixed flame is first calculated using Cantera [44] for a stoichiometric mixture (computed using Bilger's definition [45]) at the initial pressure and temperature of the studied spray. The length of the 1D domain is 0.2 mm allowing to stabilize the 1D premixed flame in the middle of the domain without interactions with auto-ignitions ahead of it as discussed in [46] (this problem is also known as the ”cold boundary problem” [47]). The thermal flame thickness was hereby found to be 32 µm.

In a second step, the same 1D flame simulation was performed with AVBP using different spatial resolutions. This allowed to show that a spatial resolution of 6 µm was sufficient to solve for all species present in the ARC scheme and to reproduce the CANTERA findings.

4. Analysis tools for DNS

An important issue to analyze the stabilization mechanisms is to build adapted post-processing tools for the DNS results. To this purpose, we first developed a method for tracking the temporal variations of LOL, which then exploited for identifying four different reaction zone topologies of importance for the flame stabilization.

4.1. LOL definition

For each instantaneous DNS solution, two distinct LOL are identified: the LOL for the flame base located above ($R > 0$, see Fig. 1) and below ($R < 0$) the injector. This decomposition was possible because the upper flame branch interacts weakly with the lower one, and presented the advantage of increasing the number of lift-off tracked. Here, we chose to track the lift-off according to a double criterion: First, the local heat release rate needs to exceed a threshold value of $\dot{\omega}_{T,crit} = 4 \times 10^{11} W/m^3$, corresponding to 83 % of the maximum $\dot{\omega}_T$ reached in the corresponding premixed stoichiometric laminar flame. Second, if the first criterion is met, the temperature must exceed a value of $T_{crit} = 1900K$ in a region of 0.15 mm around the point closest to the injector for which the first criterion is met. This double criterion is required to eliminate events where heat release peaks occur for a short period of time, but for which the kernel fails to grow, indicating that a minimum flame radius is not reached. The lift-off is then defined as the closest point to the nozzle, meeting this double criterion, and allows to compute the LOL, which is the distance between the lift-off and the fuel injector. Following the methodology proposed in [19], the LOL are

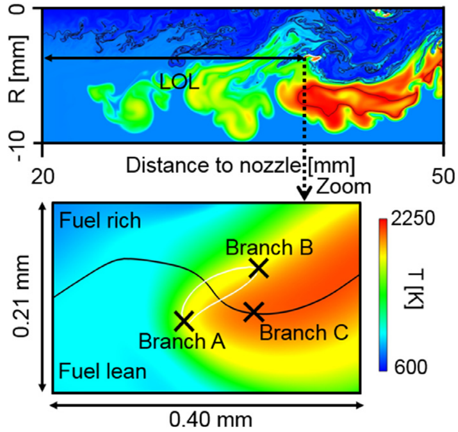

Fig. 4. Instantaneous temperature profile of the stabilized flame (above the injector: $R < 0$) showing a triple flame. The bottom image is a zoom around the lift-off found in the upper image. The black line represents the stoichiometric line. The white line shows $4 \times 10^{11}\,W/m^3$ iso-contour of heat release rate.

tracked between 3 and 12 ms After the Start of Injection (ASI) with a time resolution of 0.01 ms leading to 1,802 (901 × 2) LOL.

4.2. Identification of the reaction zone topologies

Once the tracking of the evolution of the lift-off is made possible, an analysis of the local reaction zone structure in its neighborhood allows identifying different events linked to the stabilization.

4.2.1. Reaction zone topologies during auto-ignition events

Auto-ignition is identified by a discontinuity of the LOL time-tracking leading to very rapid upstream displacements of the LOL, as observed in a previous experimental study [19]. Therefore, in this paper, auto-ignition is defined by the following expression: $-\Delta\text{LOL} \,/\, \Delta t > 80$ m/s, where ΔLOL and Δt are the LOL and time variation between two instants (here, Δt is set to 0.01 ms). We found that the identification process is fairly insensitive to the value of the threshold. In the following, a value of 80 m/s has been chosen.

In order to provide a deeper understanding of the auto-ignition events, two types of auto-ignitions were identified: isolated auto-ignition (AI-I), and auto-ignition assisted by burnt gases (AI-BG). An AI-I is identified as an auto-ignition event occurring in fresh gases, so without being affected by any surrounding burnt gases. The appellation “isolated” is given if the temperature is below T_{crit} within the edge (0.04 mm thick) of a square box of 3.8 × 3.8 mm centered at the lift-off. Otherwise, (if $T_{crit} > 1900K$) the appellation ”assisted by burnt gases” is given, which corresponds to an auto-ignition event close to a high-temperature zone.

4.2.2. Reaction zone topologies during continuous evolution of the lift-off

In the absence of auto-ignition events or flame extinctions, the lift-off has been divided into two reaction zone topologies: Triple Flames (TF) and Lean/Rich Reaction Zones (L/R RZ).

TF can be identified for certain LOL, as shown in Fig. 4, where a zoom on the flame base reveals the existence of the conventional branches of a TF [4,48]: branch A is a lean premixed flame, branch B designates a rich premixed flame, and branch C, a diffusion flame. The TF are detected by post-processing the mixture fraction, temperature, and heat release rate fields within a square area of 0.3 × 0.3 mm^2 around the flame base location. The conditions used to detect a TF are:

- The TF must have two intersection points between z_{st} and $\dot{\omega}_{T,crit}$.
- The TF must propagate towards fresh gases on the stoichiometric line where $T < T_{crit}$, while the downstream branch C is defined as a stoichiometric line where $T > T_{crit}$.
- One branch of the reaction zone must be on the lean side ($z_{branchA} < z_{st}$), while the other branch needs to be on the rich side ($z_{branchB} > z_{st}$).

L/R RZ is the name given to the reaction zones which are not triple flames during continuous evolutions of the LOL. These zones can be identified just after a jump of the LOL attributed to an AI-I. In this case, the lift-off is first detected on the fuel rich side as shown in Fig. 5-(a). Similar results have been shown in [49] by performing unsteady Reynolds averaged Navier-Stokes simulations of Diesel spray flames, where the ambient pressures are 42 bar and 85 bar. The authors have found that the high-temperature flame first appears on the fuel rich side in the region where the scalar dissipation rate is low and the residence time is long. In the present DNS, these regions are mixture pockets observed at the jet periphery, where the flow velocity is relatively low. Due to thermal expansion, the heat release rate threshold then moves on the fuel lean side as shown in (a'). Lastly, L/R RZ is also found after TF events when the reaction zone leaves the stoichiometric line as displayed in (b) with the arrows indicating the displacement of the TF out of the stoichiometric line, resulting in a lean reaction zone (b').

5. Comparison between DNS and experiments

In order to assess the accuracy/validity of the DNS, a comparison between experiments and the DNS when the flame has reached a quasi-steady state is proposed. Figure 6 shows a snapshot of mixture fraction (z) and formaldehyde mass fraction (Y_{CH_2O}) fields at 3.53 ms ASI. The high-temperature flame can be visualized through the iso-lines of temperature (Fig. 6-top) or OH mass fraction (Fig. 6-bottom). As in the experiments (Fig. 1-top), the flame is lifted between 30 and 40 mm from the injector. Figure 6, for $R > 0$, shows a detached auto-ignited kernel upstream of the main flame which suddenly decreases the LOL as observed experimentally [5–7,19]. Moreover, as observed in [19,50,51], DNS predicts formaldehyde upstream the high-temperature reaction zone.

Additionally, a comparison of the cool-flame structure (identified by CH_2O) between experiments and DNS is proposed through averaged images in Fig. 7-(a). CH_2O is experimentally measured with 355 LIF (laser generating a 100 mJ laser beam at 355 nm and collected between 400 and 490 nm). The experimental CH_2O averaged image is built by averaging 10 images collected at 4 ms, when the flame has reached a ”quasi-steady” state. The DNS field of Y_{CH_2O} is averaged between 3 and 12 ms. A comparison between experiments and DNS shows that the upstream location of the stabilized cool-flame is similar. However, the DNS CH_2O levels are lower than experimental levels in the center jet of the DNS. Nevertheless, the lack of CH_2O in the center jet is expected not to have a strong impact on the stabilization mechanisms since the high-temperature flame is stabilized at the jet periphery, where CH_2O is correctly predicted.

Figure 7-(b) also shows a comparison of the high-temperature flame between experiments (OH^*) and DNS (OH). The OH^* image is generated by temporal (between 1.35 and 3 ms) and ensemble (10 realizations) averaging using data, collected by high-speed OH^* chemiluminescence imaging at 60 kHz. The DNS field of Y_{OH} is averaged between 3 and 12 ms. Regarding the high-temperature flames, the difference of signal collected in the center jet between the experiments and the DNS is attributed to the line of sight 3D collection of OH^* chemiluminescence. Indeed, OH PLIF has shown OH species at the jet periphery [50] as observed in the DNS. OH^*

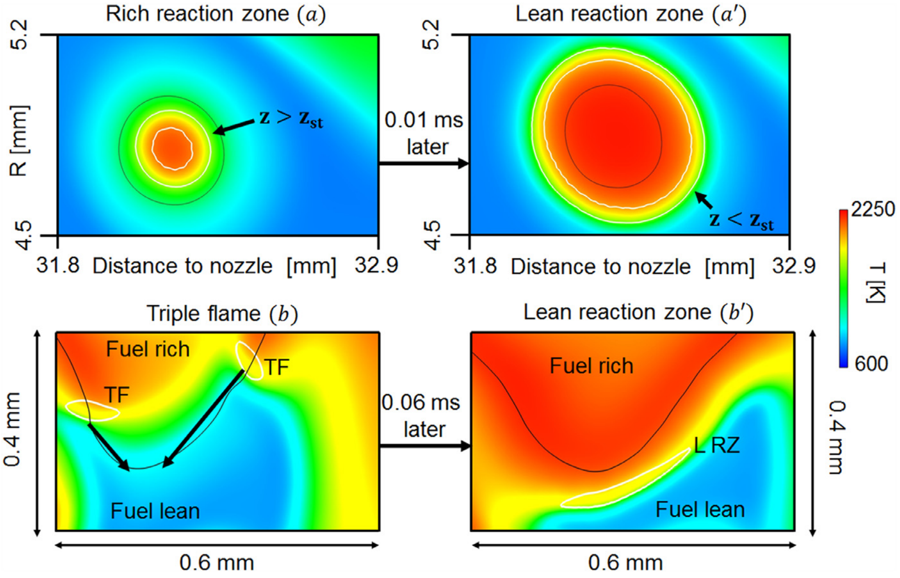

Fig. 5. (a) and (a'): two different instantaneous views illustrating a rich reaction zone (a) and a lean reaction zone (a') after an auto-ignition event. (b) and (b'): time sequence showing triple flames leaving the stoichiometric line. The black line represents the stoichiometric line. The white line shows the contour of heat release rate of $4 \times 10^{11}\, W/m^3$.

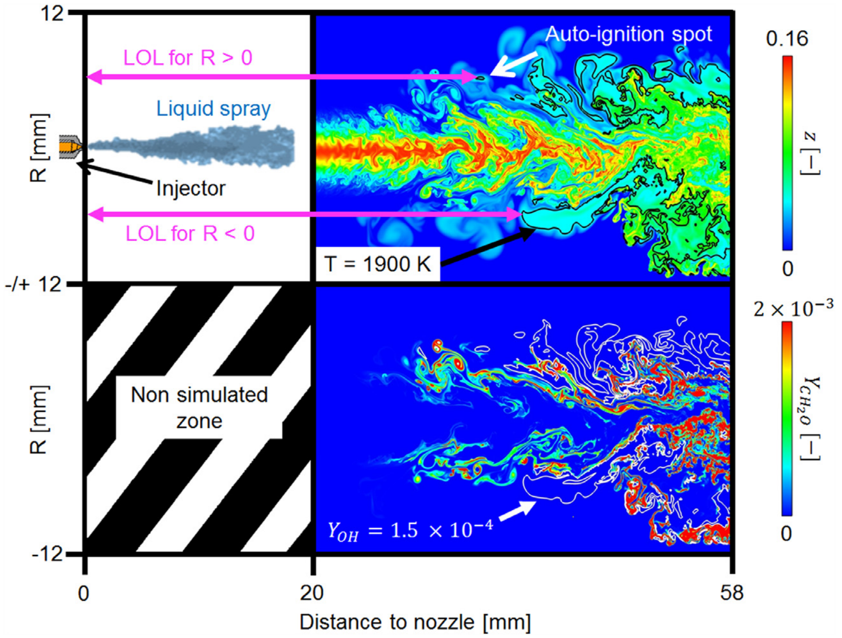

Fig. 6. DNS fields at 3.53 ms After the Start of Injection (ASI). Top image: mixture fraction field with an iso-line of temperature at 1900 K (black line). Bottom image: formaldehyde field with an iso-line of OH mass fraction at 1.5×10^{-4} in white.

chemiluminescence image allows to visualize the average LOL of the high temperature flame, which corresponds to the DNS results.

In conclusion, even if differences between experiments and DNS exist, the simulation reproduces the main features observed experimentally:

- The upstream position of the low- and high-temperature flame, in the DNS, is similar to the experiments.
- The DNS reproduces the presence of auto-ignited kernels upstream of the high-temperature flame. Such events are responsible for high LOL variation, which have been identified as a capital parameter in the flame stabilization [19].

6. Analysis of stabilization mechanisms

6.1. LOL tracking with reaction zone topologies

A description of the flame stabilization mechanisms is proposed using the time-tracking of the different reaction zone topologies identified at the lift-off defined in Section 4.2. Figure 8 presents the LOL evolutions where, for the sake of clarity, only 3 ms are displayed, but the full physical time simulated is 12 ms. Each discrete point in time, obtained from analyzing the DNS every 0.01 ms, is identified by a specific symbol for each of the four topologies defined in Section 4.2.

The same two main characteristic behaviors, observed experimentally in [19] (Fig. 5), are also reproduced in the DNS: auto-

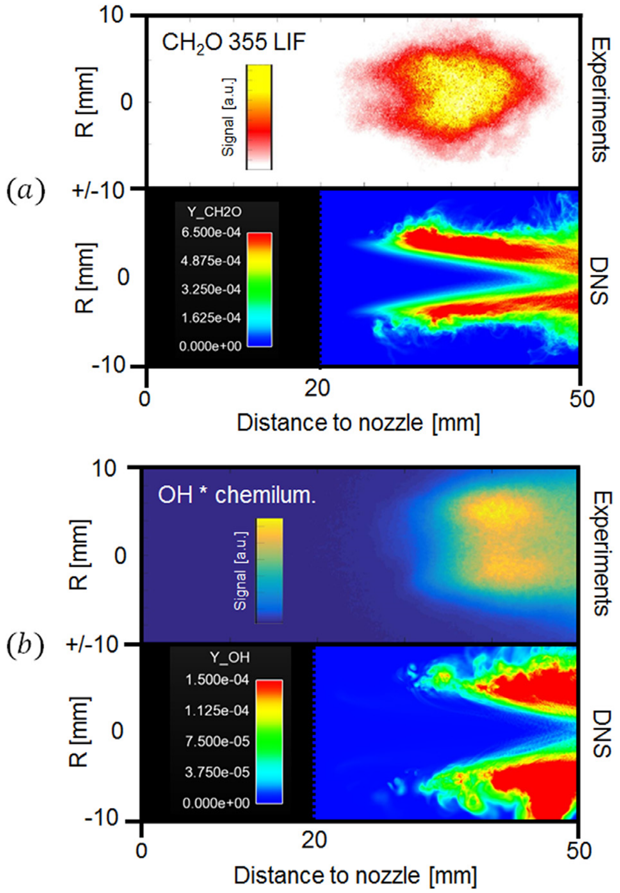

Fig. 7. (*a*): Average images of the high-temperature flame visualized by OH^* and OH species. (*b*): Average images of the cool-flame visualized by CH_2O species. The experimental data are generated using the experimental setup presented in [19].

ignition events (also named Event A) and continuous evolutions of the LOL, which are mainly downstream evolutions of the lift-off named Evolutions B.

Figure 9-(*a*) allows to illustrate the LOL time-tracking during an auto-ignition event. At t_0, the flame is stabilized far from the injector, then, at t_1, an auto-ignition occurs (AI-I or AI-BG), which brutally decreases the LOL. As shown in Fig. 8, at 4.5 ms (AI-BG) or at 4.5 ms (AI-I), auto-ignitions can decrease the LOL by 10 mm in 0.01 ms, and quasi-systematically Evolution B starts after these events.

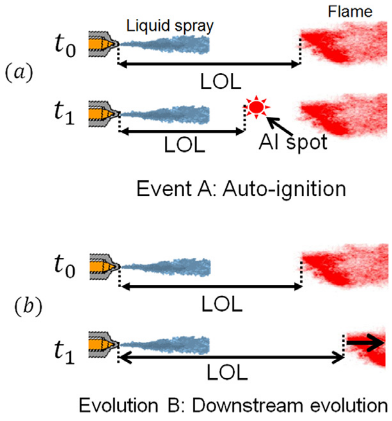

Fig. 9. (*a*): auto-ignition event, also named Event A, occurring at t_1. (*b*): downstream evolution, between t_0 and t_1, also named Evolution B.

Figure 9-(*b*) illustrates Evolution B, where at t_1, the flame has been convected downstream. An example of downstream evolution is proposed in Fig. 8, between 3 and 3.26 ms, where the lift-off is mainly identified as TF.

This decomposition into auto-ignition and downstream evolution implies that, if no new auto-ignition occurs, bringing the flame closer to the injector, the flame cannot sustain the flow and is, therefore, blown.

6.2. Analysis of Event A

Focusing on Event A, a statistical analysis at the lift-off (between 3 and 12 ms) shows that 69 % of the auto-ignition events come from AI-BG (thus 31 % from AI-I). This demonstrates the leading role of high temperature burnt gases, which can trigger auto-ignitions and help to stabilize the flame. This observation confirms the hypothesis of Pickett et al. [6] that high temperature burnt gases reservoirs at the jet periphery could be an important factor in the flame stabilization.

First, focusing on AI-I, Figure 10 shows a sequence of a stoichiometric pocket convected at the jet periphery (radially between 3.5 and 5.0 mm from the center line). It starts 0.19 ms before the AI-I and finishes when the AI-I is detected. It has been constructed starting from the third image (corresponding to the time at which an AI-I occurs, named t_{AI-I}), and exploring the DNS backward in time to see where this event actually starts. The three plots under the images represent the CH_2O and OH mass fraction profiles along the red dotted line (1 mm long) for different timings. At, 0.19 ms before AI-I, Y_{CH_2O} is very small and Y_{OH} almost inexis-

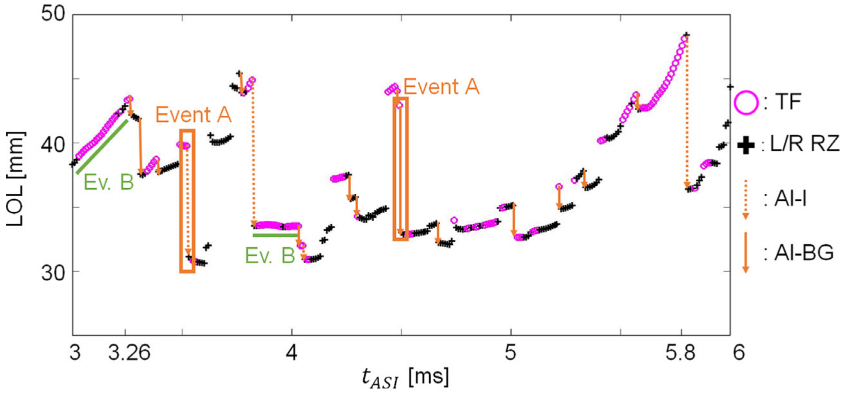

Fig. 8. LOL time-tracking with the detection of Triple Flames (TF), Lean/Rich Reaction Zones (L/R RZ), Isolated Auto-Ignitions (AI-I) and Auto-Ignitions Assisted by Burnt Gases (AI-BG) at the lift-off for $R > 0$.

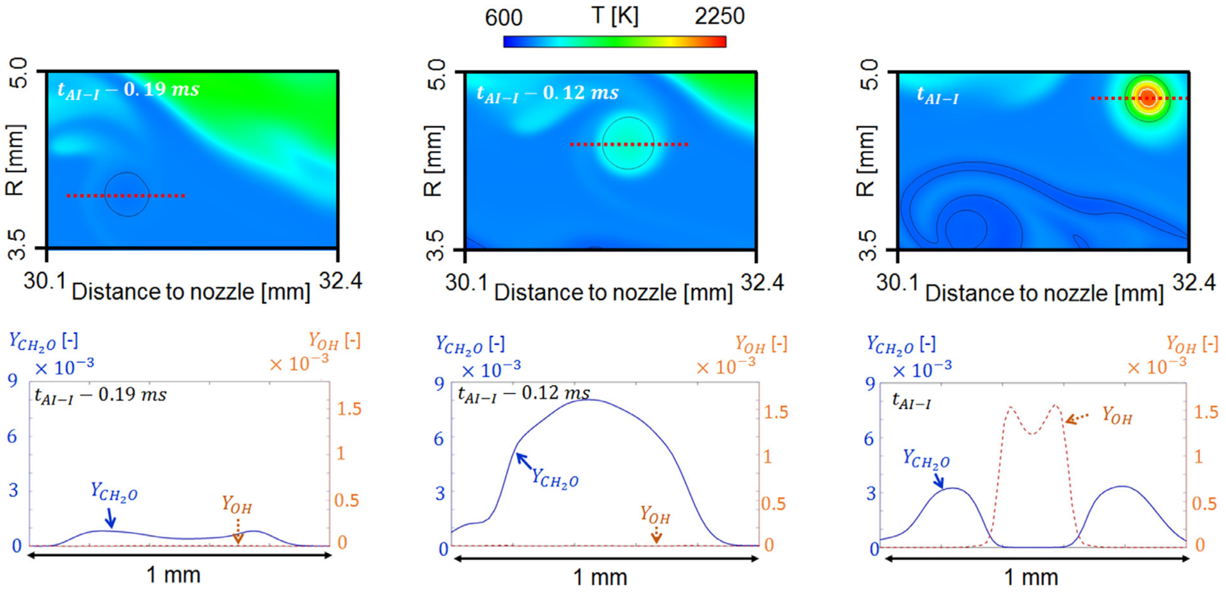

Fig. 10. Image sequence illustrating an isolated auto-ignition (AI-I) at the lift-off. The black line represents the stoichiometric line and the white line shows the contour of heat release rate of $4 \times 10^{11} W/m^3$ (top images). The three bottom plots show OH and CH_2O mass fraction profiles along the red dotted line (measuring 1 mm long) shown on the top image sequence.

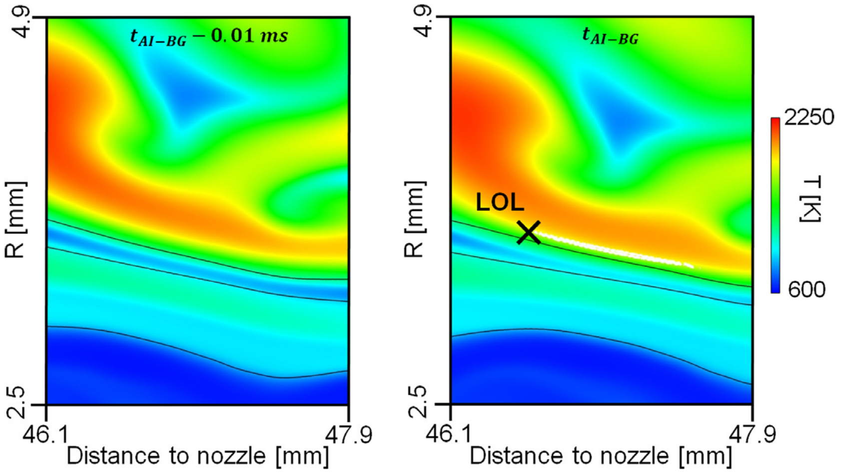

Fig. 11. Image sequence leading to an AI-BG event. The black line represents the stoichiometric line. The white line shows $4 \times 10^{11} W/m^3$ iso-contour of heat release rate.

tent. At, 0.12 ms before AI-I, Y_{OH} is still almost inexistent. However, Y_{CH_2O} raises to a maximum of 8×10^{-3} (compared to 1.8×10^{-3} in a stoichiometric premixed flame). According to [23], $t_{AI-I} - 0.12$ ms corresponds to the time between the 1^{st} and the 2^{nd} stage of ignition because of the large amount CH_2O, the significant rise of temperature and the lack of OH. At t_{AI-I}, an AI-I is detected, Y_{OH} has risen up to 1.5×10^{-3} at the center of the stoichiometric pocket, where the temperature is maximum, and CH_2O is totally consumed. This instant corresponds to the 2^{nd} stage of ignition, where heat release and temperature become high enough to define the lift-off, according to our double criterion (described in Section 4.1). In conclusion, the different stages, shown between $t_{AI-I} - 0.19$ ms and t_{AI-I}, follow the same well-known steps than auto-ignition in 0D homogenous reactor configurations.

Figure 11 illustrates an AI-BG event, where combustion starts near a zone of hot gases: auto-ignition occurs between the stoichiometric line and a burnt gases pocket, without presenting the two stages observed for AI-I. In this case, burnt gases pockets move, due to the flow convection, and when they are close enough to the stoichiometric line, they trigger AI-BG.

6.3. Analysis of Evolutions B

An illustration of Evolution B is proposed in Fig. 12. At 3.03 ms ASI, a TF is detected at the lift-off, then 0.23 ms later, the LOL has increased by 4.4 mm (still defined as a TF) showing that this flame is convected downstream. The proportion of TF, L/R RZ is almost the same during Evolution B: 45 % TF and 55 % L/R RZ. It indicates that edge-flames must be taken into account to correctly model spray combustion under Diesel conditions as suggested in [10,17,20–23].

In our case, the edge-flames of interest are TF located at the lift-off. The question is to assess whether or not the TF propagation is balancing the flow. An analysis consists in a comparison between the orientation of the TF propagation and, first, the spray axis, then, the local flow. Figure 13-(a) shows the definition of the instantaneous angle θ_{TF} and θ_{flow} used to compare these directions against the axis. Figure 13-(b) shows two series of angles observed in the DNS: one above the injector (marked by the + exponent), the other below (marked by the - exponent). In both cases, the TF are mainly oriented towards the center line. None of these two

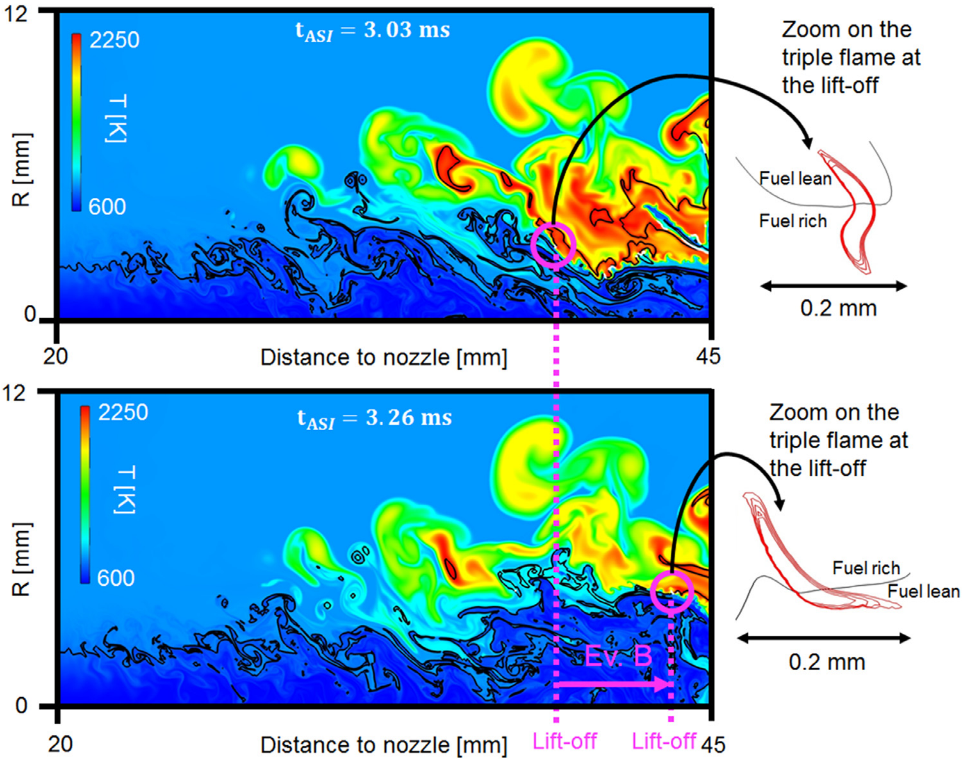

Fig. 12. Instantaneous temperature fields showing Evolution B between 3.03 and 3.26 ms ASI. Black line: stoichiometric line. The triple flames detected at the lift-off are zoomed, and displayed on the right of the images. Iso-lines of heat release rate between $3.7 \times 10^{11} W/m^3$ and $4.3 \times 10^{11} W/m^3$ are displayed in red on the zoomed images.

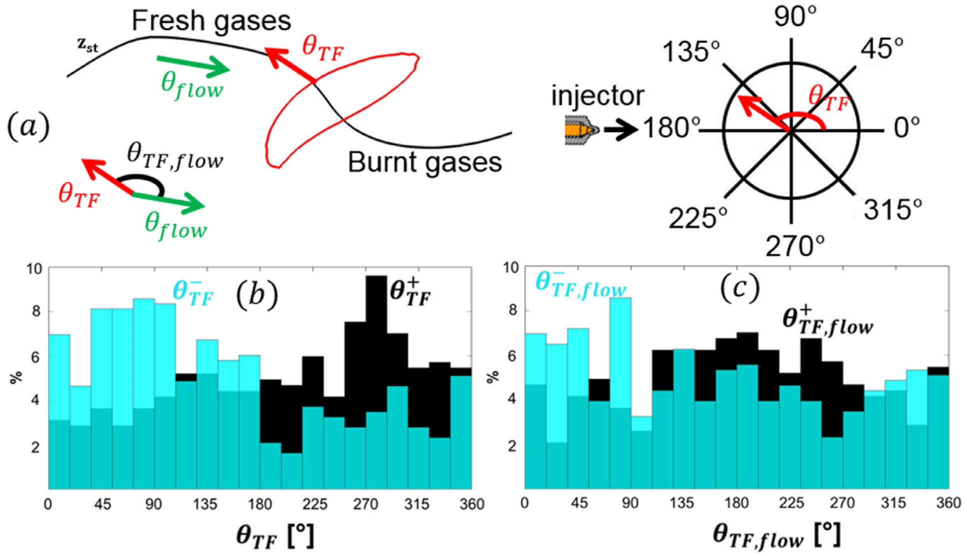

Fig. 13. (*a*): cartoon of a triple flame propagating along z_{st}. The red solid line represents the $\dot{\omega}_{T,crit} = 4 \times 10^{11} W/m^3$ iso-line. The red arrow shows the triple flame propagation direction (θ_{TF}) while the green arrow shows the flow direction (θ_{flow}). (*b*): histograms of θ^+_{TF} and θ^-_{TF}. (*c*): histograms of $\theta^+_{TF,flow}$ and $\theta^-_{TF,flow}$ (right) (For interpretation of the references to color in this figure legend, the reader is referred to the web version of this article.).

histograms show a preferential direction around 180°, which indicates that statistically, TF do not propagate upstream. Naming the angular difference between the TF propagation direction and the upstream flow $\theta_{TF,\ flow}$ (as shown in Fig. 13-(*a*)), an histogram can be built and is shown in Fig. 13-(*c*). The dispersed distribution of $\theta^+_{TF,flow}$ and $\theta^-_{TF,flow}$ shows the TF do not have a preferential propagation direction with respect to the flow.

Since the flame stabilization is defined by axial displacement of the flame, a comparison between the axial flow velocity at the lift-off ($U_{X,\ flow,\ LO}$) and the absolute axial flame front speed relative to a fixed reference (S_a) is proposed trough the ratio $U_{X,\ flow,\ LO}/S_a$. S_a is defined as the temporal variation of LOL. In order to eliminate spurious behaviors, only triplets of consecutive LOL values with correlation coefficient $r^2 > 0.98$ are considered. $U_{X,\ flow,\ LO}$ are computed by averaging the corresponding three instantaneous axial flow velocities at the lift-off.

Figure 14-(*a*) shows a histogram of the ratio $U_{X,\ flow,\ LO}/S_a$ computed between 3 and 12 ms for both positive and negative radial coordinates of TF at the lift-off. The mean value of this distribution is 0.83, which indicates that S_a is statistically the same or-

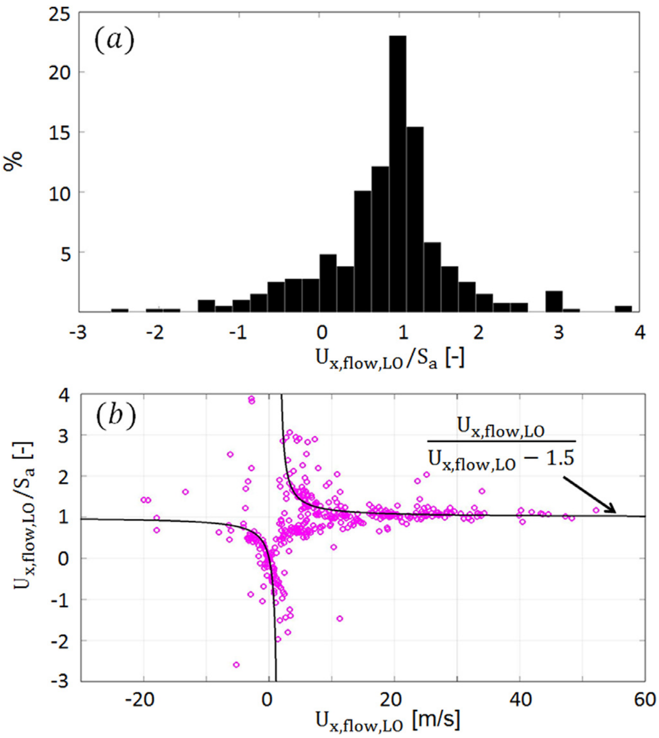

Fig. 14. Both graphics have been constructed from triple flames data at the lift-off for $R > 0$ and $R < 0$. (a): Histogram of the ratio $U_{X,\ flow,\ LO}/S_a$. (b): symbols show $U_{X,\ flow,\ LO}/S_a$ as a function of $U_{X,\ flow,\ LO}$, while the black curve displays $U_{X,flow,LO}/(U_{X,flow,LO} - 1.5)$ as a function of $U_{X,\ flow,\ LO}$.

der of magnitude than $U_{X,\ flow,\ LO}$, and thus that the flow controls the evolution of the LOL. However, this analysis can be further detailed. The ratio $U_{X,\ flow,\ LO}/S_a$ is plotted as a function of $U_{X,\ flow,\ LO}$ in Fig. 14-(b). It appears that for $U_{X,\ flow,\ LO} > 15$, the ratio is very close to 1, meaning that S_a is governed by the flow. In order to interpret the points corresponding to $U_{X,\ flow,\ LO} < 15$, DNS of flames under Diesel-like conditions [17,23] have indicated that the order of magnitude of the TF displacement speed S_d is between 1 and 2 m/s. Assuming $S_d = 1.5$ m/s, these TF should, therefore, correspond to a curve $U_{X,flow,LO}/(U_{X,flow,LO} - 1.5)$. Figure 14-($b$) indeed shows that the points corresponding to $U_{X,\ flow,\ LO} < 15$ lie very close to this curve.

Thus, there are regions where the flow velocity is of the same order of magnitude than S_d, i.e. regions where the TF can resist to the convection by the fresh gases flow. However, in most regions of the jet, the flow has a much higher velocity than S_d, and therefore Evolution B is governed by the local flow velocity. This conclusion is different from what is observed for lifted diffusion flames under non-autoignitive conditions [2–4,48,52], for which the flame is locally stabilized by an equilibrium between flow velocity and S_d.

Not shown here, plotting a similar histogram to the one, shown in Fig. 14-(a) for the L/R RZ, shows that Evolution B for these zones is also governed by the local flow velocity.

7. Conceptual model of flame stabilization

The findings from the presented simulations and from optical diagnostics allow proposing a conceptual model for the stabilization of a Diesel-type ACDF flame. To this purpose, Figure 15 shows an idealized cross-sectional slice through the mid plane of a spray flame. Only the top branch of the jet is displayed ($R > 0$). Labelled (a) to (f), six basic local reaction zone topologies are shown on relation to an idealized instantaneous stoichiometric line in the downstream gaseous part of the jet.

As found above, the key necessary stabilization mechanism is auto-ignition. Two different types of auto-ignition can be found, both pertaining to Event A introduced above: isolated spontaneous auto-ignition, leading to the local topology (a); and auto-ignition assisted by burnt gases, corresponding to the local topology (b). Depending on whether an (a) or (b) topology creates an Event A, two different stabilization scenarios can be distinguished in Fig. 15:

Scenario 1 starts with an isolated auto-ignition spot (a) localized in a stoichiometric pocket detached from the main jet. This results in an upstream jump of LOL as seen in Fig. 8 (dotted arrows). The lift-off is first detected on the fuel-rich side of the local mixture pocket for a few microseconds as displayed in Fig. 5-(a). The resulting reaction zone growths in size, and as a result of thermal expansion, the LOL is detected on the fuel-lean side of the mixture pocket as shown in Fig. 5-(a'), corresponding to a local topology of type (d) in Fig. 15. During the transition from (a) to (d), the

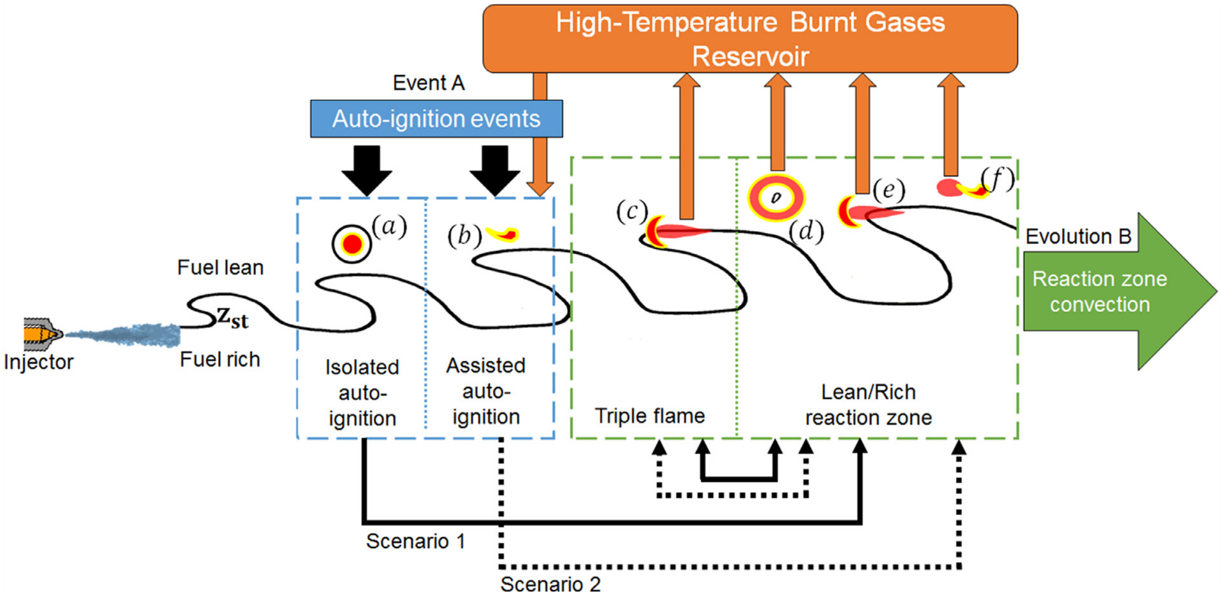

Fig. 15. Sketch illustrating the conceptual model of flame stabilization under Diesel condition derived from optical diagnostics and DNS.

lift-off axially remains relatively stable due to thermal expansion that opposes to convection by the flow [53]. At the same time, the resulting burnt gases feed high-temperature reservoirs situated in external low-velocity or recirculation regions of the jet. Such burnt gases reservoirs remain axially quite stable, and can ultimately lead to topologies (b) at the origin of scenario 2 (see below). Topologies of type (d) can then either extinguish, or reach the stoichiometric line, leading to the appearance of a TF corresponding to topology (c). According to Section 6.3, the absolute flame speed of the TF is mainly governed by the flow velocity, and the TF is convected downstream resulting in Evolution B. During this evolution, the TF also feeds burnt gases to the high-temperature reservoirs because of the displacement of their diffusion flame branch.

Finally, a TF can deviate from the stoichiometric line, leading to the appearance of a topology of type (e), corresponding to a lean or rich reaction zone as shown in Fig. 5-(b'). Transitions between topologies (e) and (c) can happen in both directions until a new auto-ignition occurs or local extinction is encountered.

Scenario 2 starts with a topology of type (b), i.e. an assisted auto-ignition by burnt gases coming from high-temperature reservoirs that are fed by the topologies (c) − (f). Topology (b) mainly transitions to (f) which corresponds to fuel-lean reaction zones as illustrated in Fig. 11. Unlike topology (d), the reaction zones of topology (f) are surrounded by burnt gases which limit the thermal expansion. They are thus growing slower, and are convected downstream by the flow following Evolution B. During this evolution, they feed burnt gases to the high-temperature reservoirs, which, thus, potentially facilitating the appearance of future scenarios 2. Topologies (f) can also reach a stoichiometric line and form TF corresponding to topology (c). The latter also feeds burnt gases to the high-temperature reservoirs, and follows an Evolution B.

In summary, auto-ignition is indispensable for allowing to stabilize a spray flame under Diesel-like conditions. Auto-ignition events appear intermittently in the upstream part of the jet, leading to the strong discontinuities in LOL observed in experiments and simulations. In-between such auto-ignitions, the leading edge of the reaction zones that can have any of the four topologies (c) - (f) are convected downstream by the strong velocities resulting from the high-pressure liquid jet. Even if these secondary topologies are ultimately blown, they allow sustaining combustion by feeding burnt gases to high-temperature reservoirs situated at the periphery of the jet. These reservoirs, indeed, facilitate the appearance of upstream auto-ignition by burnt gases, which combined with spontaneous auto-ignition allows intermittent strong reductions of the LOL, which ultimately allows an overall stabilization of the flame.

The flame stabilization mechanism is a coupling between the main mechanism auto-ignition and secondary mechanisms linked to the downstream convection of reaction zones. The two mechanisms are linked by the high temperature burnt gases reservoirs at the jet periphery, confirming the hypothesis proposed in [6].

8. Conclusion

This joint experimental/numerical study focused on the stabilization mechanisms of Autoignitive Conditions Diffusion Flames (ACDF) created when a high speed fuel jet was injected into hot air. Starting from experimental observations of n-dodecane jets into hot air, a specific DNS was built to elucidate mechanisms which control the LOL (Lift-Off Length). The analysis of the DNS showed that two types of mechanisms control the flame stabilization: auto-ignition events, where the LOL jumped rapidly to small values, followed by evolutions where the flames, created by auto-ignition events, were convected downstream by the flow without significant flame propagation effects. To obtain these results, a post-processing methodology to extract information, from DNS fields, was derived. The main conclusion is that auto-ignition was the key stabilization mechanism, while triple flames, even if they exist, had insufficient propagation speeds to contribute to the flame stabilization. These flames were visible in multiple points of the flame brush, but they cannot be expected to provide a stabilization mechanism. Future studies should further explore the behavior of the presented conceptual model according to test condition variations (e.g. ambient temperature, and injection pressure variation). Finally, a Diesel engine environment is wall bounded and characterized by jet-jet interactions in the context of a swirling flow [54,55]. These differences with the presently studied unbounded isolated spray could impact the stabilization mechanisms and their interactions. This would have to be explored in future experimental and simulation work.

Acknowledgments

This project was granted access to the HPC resources of CINES and TGCC under allocation no. A0032B06672 from the GENCI (Grand Equipement National de Calcul Intensif) DARI program. The help of Dr. Gabriel Staffelbach to construct the AVBP mesh is gratefully acknowledged. We also thank Dr. Ahmad El Sayed for his assistance to reduce the chemical mechanism.

Appendix 1

The inlet NSCBC [35] boundary condition (left edge of the computational domain) is addressed imposing radial profiles of mean axial velocity (Eq. (1)), temperature (Eq. (2)), mass fraction species (Eq. (3)) and synthetic isotropic turbulence (Eq. (4)):

$$\begin{cases} U_X(R) = U_X^{max}\exp(-R^2/2\sigma_1^2) + U_{coflow} \\ U_X^{max} = 80\ m/s \end{cases} \tag{1}$$

$$T(R) = T_{amb} + (600 - T_{amb})\exp(-R^2/\sigma_1^2) \tag{2}$$

$$\begin{cases} Y_{nC_{12}H_{26}}(R) = 0.153\exp(-R^2/\sigma_1^2) \\ Y_k(R) = (1 - Y_{nC_{12}H_{26}})Y_k^0 \quad \text{with} \quad k = N_2, O_2, CO_2, H_2O \end{cases} \tag{3}$$

$$\begin{cases} U_{RMS}(R) = U_{RMS}^{max}\exp(-(R-\mu)^2/\sigma_2^2) + U_{RMS}^{max}\exp(-(R+\mu)^2/\sigma_2^2), \\ U_{RMS}^{max} = 7\ m/s \end{cases} \tag{4}$$

where:

- R is the radial coordinate
- σ_1, σ_2 and μ are constant respectively equal to 1.8, 1.4 and 1.7 mm
- U_{coflow} is a co-flow used to avoid negative axial velocity on the inlet boundary condition set to 1 m/s
- T_{amb} is the ambient temperature (800 K)
- $Y_{N_2}^0$, $Y_{O_2}^0$, $Y_{CO_2}^0$, $Y_{H_2O}^0$ are given in Table 1

References

[1] S. Karami, E.R. Hawkes, M. Talei, J.H. Chen, Mechanisms of flame stabilisation at low lifted height in a turbulent lifted slot-jet flame, J. Fluid Mech. 777 (2015) 633–689.
[2] H. Phillips, Flame in a buoyant methane layer, Symp. (Int.) Combust. 10 (1965) 1277–1283.
[3] P.N. Kioni, B. Rogg, K. Bray, A.L. nán, Flame spread in laminar mixing layers, Combust. Flame 95 (1993) 276–290.
[4] G.R. Ruetsch, L. Vervisch, A.L. nán, Effects of heat release on triple flames, Phys. Fluids 7 (1995) 1447–1454.
[5] L.M. Pickett, D.L. Siebers, C.A. Idicheria, Relationship between ignition processes and the lift-off length of diesel fuel jets, SAE Technical Paper (2005). 2005-01-3843.

[6] L.M. Pickett, S. Kook, H. Persson, O. Andersson, Diesel fuel jet lift-off stabilization in the presence of laser-induced plasma ignition, Proc. Combust. Inst. 32 (2009) 2793–2800.
[7] C. Pauls, G. Grünefeld, S. Vogel, N. Peters, Combined simulation and OH-chemiluminescence measurements of the combustion process using different fuels under diesel-engine like conditions, SAE Technical Paper (2007). 2007-01-0020.
[8] Y. Pei, E.R. Hawkes, M. Bolla, S. Kook, G.M. Goldin, Y. Yang, S.B. Pope, S. Som, An analysis of the structure of an n -dodecane spray flame using TPDF modelling, Combust. Flame 168 (2016) 420–435.
[9] C. Gong, M. Jangi, X.S. Bai, Diesel flame lift-off stabilization in the presence of laser-ignition, Combust. Theor. Model. 19 (2015) 696–713.
[10] A. Krisman, E.R. Hawkes, M. Talei, A. Bhagatwala, J.H. Chen, Polybrachial structures in dimethyl ether edge-flames at negative temperature coefficient conditions, Proc. Combust. Inst. 35 (2015) 999–1006.
[11] D.L. Siebers, B. Higgins, L.M. Pickett, Flame lift-off on direct-injection diesel fuel jets: Oxygen concentration effects, SAE Technical Paper (2002). 2002-01-0890.
[12] R. Payri, F.J. Salvador, J. Manin, A. Viera, Diesel ignition delay and lift-off length through different methodologies using a multi-hole injector, Appl. Energy 162 (2016) 541–550.
[13] L.M. Pickett, 2015, ECN available at http://www.sandia.gov/ecn/.
[14] D.K. Dalakoti, A. Krisman, B. Savard, A. Wehrfritz, H. Wang, M.S. Day, J.B. Bell, E.R. Hawkes, Structure and propagation of two-dimensional, partially premixed, laminar flames in diesel engine conditions, Proc. Combust. Inst. doi:10.1016/j.proci.2018.06.169.
[15] S. Deng, P. Zhao, M.E. Mueller, C.K. Law, Autoignition-affected stabilization of laminar nonpremixed DME/air coflow flames, Combust. Flame 162 (2015) 3437–3445.
[16] S. Deng, P. Zhao, M.E. Mueller, C.K. Law, Stabilization of laminar nonpremixed DME/air coflow flames at elevated temperatures and pressures, Combust. Flame 162 (2015) 4471–4478.
[17] Y. Minamoto, J.H. Chen, DNS of a turbulent lifted DME jet flame, Combust. Flame 169 (2016) 38–50.
[18] D.-H. Shin, E.S. Richardson, V. Aparece-Scutariu, Y. Minamoto, J.H. Chen, Fluid age-based analysis of a lifted turbulent DME jet flame DNS, Proc. Combust. Inst. doi:10.1016/j.proci.2018.06.126.
[19] F. Tagliante, L.-M. Malbec, G. Bruneaux, L.M. Pickett, C. Angelberger, Experimental study of the stabilization mechanism of a lifted diesel –type flame using combined optical diagnostics and laser-induced plasma ignition, Combust. Flame 197 (2018) 215–226.
[20] A. Krisman, E.R. Hawkes, M. Talei, A. Bhagatwala, J.H. Chen, Characterisation of two-stage ignition in diesel engine-relevant thermochemical conditions using direct numerical simulation, Combust. Flame 172 (2016) 326–341.
[21] A. Krisman, E.R. Hawkes, J.H. Chen, Two-stage auto-ignition and edge flames in a high pressure turbulent jet, J. Fluid Mech. 824 (2017) 5–41.
[22] A. Krisman, E.R. Hawkes, M. Talei, A. Bhagatwala, J.H. Chen, A direct numerical simulation of cool-flame affected auto-ignition in diesel engine-relevant conditions, Proc. Combust. Inst. 36 (2017) 3567–3575.
[23] G. Borghesi, A. Krisman, T. Lu, J.H. Chen, Direct numerical simulation of a temporally evolving air/n-dodecane jet at low-temperature diesel-relevant conditions, Combust. Flame 195 (2018) 183–202.
[24] B. Franzelli, E. Riber, M. Sanjosé, T. Poinsot, A two-step chemical scheme for kerosene-air premixed flames, Combust. Flame 157 (2010) 1364–1373.
[25] B. Franzelli, E. Riber, L. Gicquel, T. Poinsot, Large eddy simulation of combustion instabilities in a lean partially premixed swirled flame, Combust. Flame 159 (2012) 621–637.
[26] P. Pepiot, Automatic strategies to model transportation fuel surrogates (doctoral dissertation, Stanford University, 2008.
[27] P. Pepiot-Desjardins, H. Pitsch, An efficient error-propagation-based reduction method for large chemical kinetic mechanisms, Combust. Flame 154 (2008) 67–81.
[28] O. Schulz, T. Jaravel, T. Poinsot, B. Cuenot, N. Noiray, A criterion to distinguish auto-ignition and propagation applied to a lifted methane-air jet flame, Proc. Combust. Inst. 36 (2017) 1637–1644.
[29] O. Schulz, N. Noiray, Autoignition flame dynamics in sequential combustors, Combust. Flame 192 (2018) 86–100.
[30] T. Jaravel, E. Riber, B. Cuenot, G. Bulat, Large eddy simulation of an industrial gas turbine combustor using reduced chemistry with accurate pollutant prediction, Proc. Combust. Inst. 36 (2017) 3817–3825.
[31] R. Payri, J. García-Oliver, M. Bardi, J. Manin, Fuel temperature influence on diesel sprays in inert and reacting conditions, Appl. Therm. Eng. 38 (2012) 185–195.
[32] J.E. Dec, A conceptual model of DI diesel combustion based on laser-sheet imaging, SAE Technical Paper (1997). 970873.
[33] V. Moureau, G. Lartigue, Y. Sommerer, C. Angelberger, O. Colin, T. Poinsot, Numerical methods for unsteady compressible multi-component reacting flows on fixed and moving grids, J. Comput. Phys. 202 (2005) 710–736.
[34] P.D. Lax, B. Wendroff, Difference schemes for hyperbolic equations with high order of accuracy, Commun. Pure Appl. Math. 17 (1964) 381–398.
[35] T. Poinsot, S. Lele, Boundary conditions for direct simulations of compressible viscous flows, J. Comput. Phys. 101 (1992) 104–129.
[36] A. Smirnov, S. Shi, I. Celik, Random flow generation technique for large eddy simulations and particle-dynamics modeling, J. Fluids Eng. 123 (2001) 359–371.
[37] T. Passot, A. Pouquet, Numerical simulation of compressible homogeneous flows in the turbulent regime, J. Fluid Mech. 181 (1987) 441–466.
[38] T. Yao, Y. Pei, B.J. Zhong, S. Som, T. Lu, K.H. Luo, A compact skeletal mechanism for n -dodecane with optimized semi-global low-temperature chemistry for diesel engine simulations, Fuel 191 (2017) 339–349.
[39] S.M. Sarathy, C.K. Westbrook, M. Mehl, W.J. Pitz, C. Togbe, P. Dagaut, H. Wang, M.A. Oehlschlaeger, U. Niemann, K. Seshadri, P.S. Veloo, C. Ji, F.N. Egolfopoulos, T. Lu, Comprehensive chemical kinetic modeling of the oxidation of 2-methylalkanes from c7 to c20, Combust. Flame 158 (2011) 2338–2357.
[40] T. Lovs, D. Nilsson, F. Mauss, Automatic reduction procedure for chemical mechanisms applied to premixed methane/air flames, Proc. Combust. Inst. 28 (2000) 1809–1815.
[41] C. Ji, E. Enoch, Y.L. Wang, H. Wang, F.N. Egolfopoulos, Propagation and extinction of premixed c5-c12 n-alkane flames, Combust. Flame 157 (2010) 277–287.
[42] U. Pfahl, K. Fieweger, G. Adomeit, Self-ignition of diesel-relevant hydrocarbon-air mixtures under engine conditions, Symp. (Int.) Combust. 26 (1996) 781–789.
[43] S.S. Vasu, D.F. Davidson, Z. Hong, V. Vasudevan, R.K. Hanson, N-dodecane oxidation at high-pressures: measurements of ignition delay times and OH concentration time-histories, Proc. Combust. Inst. 32 (2009) 173–180.
[44] D.G. Goodwin, H.K. Moffat, R.L. Speth, 2015, URL: http://www.cantera.org.
[45] R.W. Bilger, S.H. Støarner, R.J. Kee, On reduced mechanisms for methane air combustion in nonpremixed flames, Combust. Flame 80 (1990) 135–149.
[46] A. Krisman, E.R. Hawkes, J.H. Chen, The structure and propagation of laminar flames under autoignitive conditions, Combust. Flame 188 (2018) 399–411.
[47] J. Hirschfelder, C. Curtiss, D.E. Campbell, The theory of flames and detonations, Symp. (Int.) Combust. 4 (1953) 190–211.
[48] L. Muñiz, M.G. Mungal, Instantaneous flame-stabilization velocities in lifted-jet diffusion flames, Combust. Flame 111 (1997) 16–31.
[49] K.M. Pang, M. Jangi, X.-S. Bai, J. Schramm, J.H. Walther, P. Glarborg, Effects of ambient pressure on ignition and flame characteristics in diesel spray combustion, Fuel 237 (2019) 676–685.
[50] N. Maes, M. Meijer, N. Dam, B. Somers, H.B. Toda, G. Bruneaux, S.A. Skeen, L.M. Pickett, J. Manin, Characterization of spray a flame structure for parametric variations in ECN constant-volume vessels using chemiluminescence and laser-induced fluorescence, Combust. Flame 174 (2016) 138–151.
[51] J.M.G. Oliver, L.M. Malbec, H.B. Toda, G. Bruneaux, A study on the interaction between local flow and flame structure for mixing-controlled diesel sprays, Combust. Flame 179 (2017) 157–171.
[52] P. Domingo, L. Vervisch, Triple flames and partially premixed combustion in autoignition of non-premixed turbulent mixtures, Symp. (Int.) Combust. 26 (1996) 233–240.
[53] M. EidiAttarZade, S. Tabejamaat, M. Mani, M. Farshchi, Numerical study of ignition process in turbulent shear-less methane-air mixing layer, Flow Turbul. Combust. 99 (2017) 411–436.
[54] C. Chartier, U. Aronsson, O. Andersson, R. Egnell, B. Johansson, Influence of jet–jet interactions on the lift-off length in an optical heavy-duty DI diesel engine, Fuel 112 (2013) 311–318.
[55] A.M. Rusly, M.K. Le, S. Kook, E.R. Hawkes, The shortening of lift-off length associated with jet-wall and jet-jet interaction in a small-bore optical diesel engine, Fuel 125 (2014) 1–14.